Video Article

Challenges in Rheological Characterization of Highly Concentrated Suspensions — A Case Study for Screen-printing Silver Pastes

Ceren Yüce[1], Norbert Willenbacher[1]

[1]Applied Mechanics Group, Institute for Mechanical Process Engineering and Mechanics, Department of Chemical Engineering, Karlsruhe Institute of Technology

Correspondence to: Ceren Yüce at ceren.yuece@kit.edu, Norbert Willenbacher at norbert.willenbacher@kit.edu

Abstract

A comprehensive rheological characterization of highly concentrated suspensions or pastes is mandatory for a targeted product development meeting the manifold requirements during processing and application of such complex fluids. In this investigation, measuring protocols for a conclusive assessment of different process relevant rheological parameters have been evaluated. This includes the determination of yield stress, viscosity, wall slip velocity, structural recovery after large deformation and elongation at break as well as tensile force during filament stretching.

The importance of concomitant video recordings during parallel-plate rotational rheometry for a significant determination of rheological quantities is demonstrated. The deformation profile and flow field at the sample edge can be determined using appropriate markers. Thus, measurement parameter settings and plate roughness values can be identified for which yield stress and viscosity measurements are possible. Slip velocity can be measured directly and measuring conditions at which plug flow, shear banding or sample spillover occur can be identified clearly.

Video recordings further confirm that the change in shear moduli observed during three stage oscillatory shear tests with small deformation amplitude in stage I and III but large oscillation amplitude in stage II can be directly attributed to structural break down and recovery. For the pastes investigated here, the degree of irreversible, shear-induced structural change increases with increasing deformation amplitude in stage II until a saturation is reached at deformations corresponding to the crossover of G' and G", but the irreversible damage is independent of the duration of large amplitude shear.

A capillary breakup elongational rheometer and a tensile tester have been used to characterize deformation and breakup behavior of highly filled pastes in uniaxial elongation. Significant differences were observed in all experiments described above for two commercial screen-printing silver pastes used for front side metallization of Si-solar cells.

Video Link

The video component of this article can be found at https://www.jove.com/video/55377/

Introduction

Front side metallization of silicon solar cells is commonly realized using traditional screen-printing. Besides stencil printing, inkjet printing and flexographic printing[1], screen-printing has been used since the 1970s for numerous printing applications[2]. It is a versatile technique and in solar cell production, it ensures simple and fast metallization at a low printing cost. However, the flow properties of screen-printing pastes have to be carefully adjusted to guarantee undisturbed, defect free processing. This is particularly challenging in solar cell metallization since narrow uniform line patterns have to be achieved. Furthermore, paste recipes have to be carefully adjusted to avoid sedimentation of the high density silver particles, phase separation and particle aggregation.

The highly concentrated conductive screen-printing pastes for front-side metallization of solar cells mainly consist of three components[3,4,5,6]: the conductive material, generally micron-sized silver particles providing good electrical conductivity[7,8]; the continuous phase, the so-called vehicle, a mixture of organic binders, solvents and additives promoting particle wetting, film formation and adhesion to the substrate that also includes additives to adjust the flow behavior, especially allowing the paste to pass the narrow screen meshes easily; and the inorganic binder (glass powder) acts as an adhesion promoter and activates the sintering process at lower temperatures.

Printing fine lines with a high aspect ratio requires silver pastes that exhibit a high yield stress and a pronounced shear-thinning behavior[9]. The high yield stress guarantees good shape accuracy and a high aspect ratio whereas strong shear-thinning and a correspondingly low viscosity at high shear rates are necessary when the paste flows through narrow mesh openings, where the paste is exposed to high shear rates estimated to be beyond 10^3 s^{-1} [10].

During the printing process, pastes are exposed to very different deformation rates and stresses. First, the paste rests on the screen; then the squeegee acts and the paste penetrates through screen openings onto the substrate. After application of the paste on the silicon wafer, structure

and viscosity must recover quickly to prohibit paste spreading on the substrate. This would reduce solar cell performances due to higher shading losses[10,11,12,13,14,15]. Interruptions, the so-called meshmarks, in printed finger lines can occur at cross points of mesh wires depending on paste rheology. The time for leveling out the meshmarks should be as long as necessary but also short enough to keep the finger line spreading as low as possible[16].

The squeegee pressure required for the paste to flow through the meshes onto the substrate has to be adjusted carefully to the high yield stress necessary to provide good shape accuracy[3,6,9,17,18]. Particles are closely packed, interact strongly and form complex structures. Accordingly, besides yield stress, shear thinning and thixotropy, various other complex flow phenomena like shear banding or avalanching may occur in such suspensions[19,20,21]. Wall slip is also crucial to concentrated suspensions[22,23,24,25]. A thin layer of liquid of lower viscosity, *i.e.* a layer depleted or free of particles is formed next to the wall[25,26,27,28,29,30,31] and may control flow through narrow gaps or channels.

So a comprehensive rheological characterization of screen-printing pastes is essential in order to improve processing properties and product features. In this study, two commercial silver pastes are characterized. These pastes exhibit substantially different printing performances. The rheological characterization of such materials is very demanding. Even the simple determination of the steady shear viscosity using a rotational rheometer is a major challenge due to wall slip, plug flow, shear banding and paste spill. Accordingly, previous studies focused on oscillatory shear measurements[10,17,21] or on the characterization of low concentrated silver pastes, so-called inks[3,6,15], for which the above-mentioned phenomena are unlikely to occur.

Protocols for a robust and meaningful characterization of the flow behavior of concentrated silver pastes can be defined with the help of video recordings. A rotational shear rheometer with a parallel-plate sample fixture is used in this study, clearly demonstrating that plug flow, wall slip, and shear banding depend on the plate roughness in a non-trivial manner.

In previous work, time-dependent development of wall slip in steady torsional flow of concentrated suspensions was examined for different plate roughness. The flow of highly concentrated suspensions of solid glass spheres in polymer binder solution was visualized and an increased plate or inner cylinder roughness prevented wall slip. However, increasing plate roughness resulted in fracture of the samples[22,25]. Fracture occurred at smaller apparent shear rates when the wall roughness was increased. The tips of the asperities of the roughened surfaces might act as stress concentration points at the plate surface, initiating fracture at shear stresses τ smaller than the yield stress τ_y[25].

Wall slip is considered to be important for the screen-printing performance of highly concentrated pastes. The paste glides through the mesh easier at higher wall slip and its deposit on the substrate is increased significantly[32]. With the help of video recordings, wall slip can be directly observed for different experimental protocols. The slip velocity can be determined directly from the angular velocity of the rotating plate using smooth plates with low roughness. But flow behavior determination on silver pastes is an inherent limitation. The suspensions are non-transparent, so optical flow field observations can only be done at the sample rim. Previous studies have tried to determine wall slip and deformation within the samples simultaneously. They observed slip below the yield stress and found a quadratic dependence of slip velocity on the shear stress. The flow behavior of transparent clay suspensions was investigated by Pignon[27] following the deformation of a dye pigment line injected into the bulk material. Persello *et al.*[26] have investigated concentrated aqueous silica suspensions. They found that increasing plate roughness to suppress wall slip does not result in a homogenous sample deformation but provoked bulk fracture. Slip and sample deformation in pastes of soft microgel particles and concentrated emulsions has been intensively discussed in a series of papers[28,29,30,31]. Fluorescent tracer particles were used to determine the flow field within these transparent samples in a cone-plate geometry. They found a characteristic slip velocity V* at the yield stress of the respective material and a power law for the increase of slip velocity with shear stress τ below τ_y. An exponent of one was found for non-adhering particles and two in the case of weak attraction between particles and wall.

In the study presented here the development of deformation and flow under controlled stress and controlled shear rate conditions is monitored. In contrast to the findings reported in Reference 25, increasing plate roughness does not result in fracture for both investigated pastes. Also, wall slip and plug flow cannot be suppressed just by increasing plate roughness. These phenomena seem to be controlled by the ratio of particle size and plate roughness. Sample spill sets in at a characteristic rotational speed presumably determined by the balance between centrifugal forces acting on and friction at the rheometer plate. However, the shear rate range in which the viscosity determination is possible can be determined, and simultaneously wall slip can be quantified. Furthermore, a capillary rheometer is used to determine the viscosity at higher shear rates relevant for the printing process.

Despite the difficulties with steady shear rheometry, well-defined oscillatory shear deformation can be implemented easily. A three-stage oscillation test (constant frequency, different oscillation amplitudes) simulates the screen-printing process[10] and allows for studying structural recovery of the paste:

In the first "pre-print" step, a small deformation is applied to determine the elastic and viscous properties at rest. The second "print" step simulates the blade coating and the paste passing the screen mesh by applying a sufficiently high deformation amplitude breaking the paste structure. In the final "post-print" step, a small deformation is applied to detect the structural recovery of the paste. The initial modulus value should be reached quickly to avoid paste spreading but not too fast to avoid meshmarks. The investigations presented here confirm that the structural recovery is incomplete as previously reported by Zhou[21]. Zhou could show that the structural change is caused by the breaking of filler clusters of filler-matrix decoupling using silver particles suspended in ethyl cellulose solution. Video recordings in this study reveal that the observed irreversible structural change is not an artefact related to the occurrence of wall slip, shear banding, plug flow or sample spill. Additionally, it is found that the degree of structural breakdown strongly depends on the deformation amplitude applied in stage two, but hardly depends on the time interval of the applied strain. This aspect was not perceived in the experiments of Zhou. The influence of the paste composition on structural breakdown and recovery will be discussed in a subsequent paper.

Finally, a method to simulate the paste behavior during screen snap-off is presented. A capillary breakup elongational rheometer and a commercial tensile tester are used to determine the stretch ratio at which the pastes break and the maximum axial force during stretching as a function of elongation velocity.

Video recordings have turned out to be indispensable for finding the appropriate measurement protocols necessary for a meaningful rheological characterization of silver pastes using parallel-plate rotational rheometry. Video data enabled the determination of shear rate and shear stress

regimes in which physically well-defined yield stress and viscosity values could be determined. The appropriate choice of plate roughness and plate separation parameters was also based on these video recordings. Experimental settings for which wall slip, pure plug flow, shear banding or sample spillage occur could be unequivocally identified. The pastes investigated here are used for front side metallization of solar cells. However, a careful video supported rheological characterization is also important for various other kinds of concentrated suspensions including high density, micron-sized particles.

Protocol

Caution: Please consult all relevant material safety data sheets (MSDS) before use. Several of the components used for the silver paste formulation are acutely toxic, carcinogenic and water-endangering substances. Please use all appropriate safety practices when handling with silver pastes (personal protective equipment — safety glasses, gloves, lab coat, full length pants, closed-toe shoes). Also working with the rheometer requires carefully work. Protect the hands from being trapped during the geometric moves to the measuring position.

1. Rotational Shear Measurements — Measurement Report

1. Apparent viscosity determination - shear rate controlled measurements
    1. Carry out rotational shear experiments using rheometer A with parallel-plate geometry (plate roughness R_q = 2 - 4 µm, plate diameter d = 25 mm). The required paste volume is 0.49 mL.
        1. Adjust the measuring settings for viscosity determination. Carry out measurements in stepwise controlled shear rate mode $\dot{\gamma}$ = 0.01 s^{-1} - 1000 s^{-1} in 40 steps. The measuring time is 1,200 s.
        2. Place the equipment for recording the measuring gap in position: camera tripod with the attached endoscopic camera, LED spotlight, and the external computer to save the recordings. Adjust the endoscopic camera settings, *e.g.* contrast and brightness of the exposure field.
        3. Just before filling up the rheometer gap, mix the sample in the reservoir so the paste is blended homogeneously.
        4. Fill up the rheometer gap with the mixed silver paste sample.
        NOTE: For a measuring gap height of h_{end} = 1 mm, first go to a gap position h_1 = 1.05 mm for removing the excess sample from the edge of the rheometer geometry. After clearing up the excess sample, change the actual gap height position from h_1 to h_{end}.
        5. To visualize the paste flow in the measuring gap, mark the paste with soot particles in a vertical line.
        6. Before starting the measurement, wait about 5 min until normal forces in the gap have decayed.
        7. Start the measurement. Start the measuring device and video recording at the same time to follow the paste in the gap and to correlate measuring settings, rheometry results, and video recordings correctly.
        8. Repeat the measurement steps 1.1.1.3 - 1.1.1.7 at least three times.
        9. Plot the apparent viscosity η_{app} vs. apparent shear rate $\dot{\gamma}_{app}$ logarithmically. Evaluate the video recordings to check the section of dominating wall slip, the section of paste deformation, and the section of sample spill. The parameter settings for which a uniform shear profile is formed can be detected easily based on the video recordings (**Figure 1**).
        NOTE: The shear stress at the edge of the plate is calculated from the recorded torque applied by the rheometer and the apparent shear rate at the edge of the plate at steady state. The apparent shear rate is referred to the angular velocity of the plate and to the gap height h at the maximum plate radius.

2. Yield stress determination — a comparison of shear stress controlled measurements with different plate roughness and vane geometry
    1. Yield stress measurement with a plate roughness of R_q = 1.15 µm.
        1. For measurements with R_q = 1.15 µm, use rheometer B with a plate diameter of d = 20 mm. The required paste volume is 0.31 mL.
        2. Adjust the measuring settings for yield stress measurement. Carry out measurements in stepwise controlled shear stress mode. Vary the shear stress between 1 Pa to 3,000 Pa in 35 steps with a total measuring time of 1,050 s.
        3. Assemble a camera tripod with the attached endoscopic camera, a LED spotlight, and the external computer with software to save the video recordings. Adjust the endoscopic camera settings, *e.g.* the contrast and brightness of the exposure field.
        4. Before filling the measuring gap with silver paste, mix the sample in its reservoir to ensure that it is blended homogeneously. Use a speed mixer (30 s at 1,000 rpm). After mixing, fill up the gap with paste.
        5. Take a small amount of the blended paste, apply it to the bottom plate of the parallel-plate rheometer and bring the upper plate to a measuring position.
        NOTE: For a measurement with gap height h_{end} = 1 mm, first go to gap position h_1 = 1.05 mm and remove the excess sample from the edge of the rheometer geometry. After clearing up the excess sample, change the actual gap height position from h_1 to h_{end}.
        6. Mark the paste in the measuring gap with soot particles in a vertical line. This enables visualization of the paste deformation and flow in the gap as well as the wall slip.
        7. Before starting the measurement, wait about 5 min until the normal force on the upper plate has vanished.
        8. Start the measurement now. Start the measuring device and video recording at the same time to follow the paste in the gap and to attribute the correct measuring settings to video recordings.
        9. Continue the measurement until the paste is spilled out of the gap.
        10. Repeat the measurement in total for three times. For each measurement, clean the measuring gap with ethanol and repeat steps 1.2.1.4 - 1.2.1.9.
        11. When the measurement is finished, plot the deformation γ vs. shear stress τ logarithmically and determine the yield stress of the medium using the tangent intersection point method[33].

    2. Yield stress measurement at a plate roughness of R_q = 2 - 4 µm.

1. For measurements with R_q = 2 - 4 µm, use rheometer A with a plate diameter of d = 25 mm. The required paste volume is 0.49 mL.
   2. Repeat the steps 1.2.1.2 - 1.2.1.11 for yield stress measurements with a plate roughness R_q = 2 - 4 µm.

3. Yield stress measurement at a plate roughness of R_q = 9 µm.
   1. For measurements with R_q = 9 µm, use rheometer B with a plate diameter of d = 20 mm and required paste volume 0.31 mL. Use double faced adhesive tape to attach pieces of sandpaper to the plates matching their diameter.
   2. Repeat the steps 1.2.1.2 - 1.2.1.11 for yield stress measurement with a plate roughness R_q = 9 µm.

4. Yield stress measurement with the vane geometry.
   1. For yield stress measurements with the vane geometry, use rheometer C.
   2. Adjust the measuring settings for yield stress measurement. Carry out the measurements in stepwise controlled shear stress mode like parallel-plate measurements in 1.2.1, 1.2.2 or 1.2.3. The parameter values are τ = 1 - 3,000 Pa in 35 steps and a total measuring time of 1,050 s.
   3. Before filling the cylindrical measuring cup with the sample, mix the sample in its reservoir to ensure that the sample is blended homogeneously. After mixing fill up the cylindrical measuring cup with 10 mL silver paste.
   4. Move the vane geometry to the measuring position and wait 5 min.
   5. Start the measurement now.
   6. For reliable results, repeat the measurement at least three times.
   7. When the measuring is finished, plot the deformation γ versus shear stress τ logarithmically and determine the yield stress using the tangent intersection point method as described above.

3. Wall slip observation
   1. Perform wall slip observations with a plate roughness R_q = 1.15 µm using rheometer B with a plate diameter d = 20 mm.
      1. Adjust the measuring settings for the wall slip determination. Carry out measurements in controlled shear stress mode for selected shear stresses between 400 Pa and 1,300 Pa and a measuring time of 300 s total.
      2. Place the equipment for recordings of the measuring gap in position: camera tripod with the attached endoscopic camera, LED spotlight and the external computer to save the recordings. Adjust the endoscopic camera settings, *e.g.* contrast and brightness of the exposure field.
      3. Before filling the measuring gap with silver paste, mix the sample in its reservoir to ensure that it is blended homogeneously.
      4. Fill up the rheometer gap with the mixed silver paste sample.
      5. Mark the paste in the measuring gap with soot particles in a vertical line for flow behavior observation.
      6. Before starting the measurement wait about 5 min until the normal forces in the gap have decayed.
      7. Start the measurement. Start the measuring device and video recording at the same time to follow the paste in the gap and to correlate measuring settings, rheometry results and video recordings correctly.
      8. Repeat the steps 1.3.1.3 - 1.3.1.7 three times for each selected shear stress.
      9. Plot the wall slip velocity v_{slip} vs. shear stress τ to display the wall slip behavior (**Figure 9**).

4. Sample spill investigation during rotational shear measurement
   1. Carry out sample spill investigation with rheometer A (plate diameter d = 25 mm and required paste volume 0.49 mL).
      1. To determine the dependency of the onset of sample spill on gap height h run steps 1.1.1.1 - 1.1.1.8 at different gap heights.
      NOTE: For a measurement with
      h_{end} = 0.2 mm first go to gap position h_1 = 0.21 mm and remove the excess sample
      from the edge of the rheometer geometry
      h_{end} = 0.5 mm → h_1 = 0.51 mm
      h_{end} = 1.0 mm → h_1 = 1.05 mm
      h_{end} = 1.5 mm → h_1 = 1.55 mm
      h_{end} = 2.0 mm → h_1 = 2.05 mm
      2. Present results as a plot of the apparent viscosity η_{app} vs. apparent shear rate $\dot{\gamma}_{app}$ for different gap heights (**Figure 10**). Determine the kink in this curve and the corresponding critical rotational speed n_{crit} and plot this vs. the gap height h (**Figure 11**).

5. Rheological characterization at high shear rates performed with capillary rheometer
   1. Perform capillary rheometer measurements using a nozzle with circular cross-section. Use a nozzle with diameter d = 0.5 mm and length L = 40 mm here. The diameter of the feed reservoir is d_{feed} = 20 mm.
      1. Adjust the measuring settings (piston velocity between 0.001 mm s^{-1} and 20 mm s^{-1}). Carry out measurements in stepwise controlled shear rate, 5 s for each measuring point.
      2. Mix the sample to ensure the paste is blended homogenously and fill up the feed reservoir with 78.5 mL silver paste.
      3. Bring the piston in measurement position and start the measurement.
      4. Calculate the shear stress from the pressure difference between sample chamber and capillary outlet. Determine this pressure drop using a 500 bar pressure transducer. Record at least 5 pressure values for each selected piston velocity.
      5. Continue the measurement until the feed reservoir is empty.
      6. Repeat the measurement (steps 1.5.1.2 - 1.5.1.5) three times.
      7. Calculate the apparent shear rate from the volumetric flow rate using piston velocity and diameter of the feed reservoir and perform the Weissenberg-Rabinowitsch correction. Calculate the wall shear stress τ_w from the measured pressure difference[34].

The apparent viscosity is then given as $\eta_{app} = \tau_w / \dot{\gamma}_{app}$. Finally, plot the apparent viscosity vs. apparent shear rate to complete the rheological characterization at high shear rates (**Figure 12**).

2. Oscillatory Shear Measurements

1. Amplitude sweep
   1. Perform amplitude sweep measurements with rheometer A using a plate diameter of d = 25 mm and a roughness R_q = 2 - 4 μm. The required paste volume is 0.49 mL.
      1. Adjust the measuring settings for amplitude sweep measurement. Carry out measurements at controlled deformation amplitude $\hat{\gamma}$ = 0.01 - 100% and a constant frequency of f = 1 Hz in 35 steps.
      2. Repeat steps 1.2.1.3 - 1.2.1.8 to complete the amplitude sweep three times. Clean the measuring gap with ethanol before each measurement.
      3. Plot the moduli G' and G" vs. the deformation amplitude $\hat{\gamma}$ logarithmically (**Figure 13**). The deformation amplitude range in which G' > G" and both moduli run parallel independent of the deformation amplitude $\hat{\gamma}$, is the linear viscoelastic regime (LVE). For structural recovery tests pick one deformation amplitude from this area for step I and step III. For step II of the subsequent three stage structural recovery test select the deformation amplitude 10% higher than $\hat{\gamma}_{cross}$ at which G' = G" to ensure a structural break down between the structural recovery tests.

2. Three stage structural recovery test
   1. Perform structural recovery tests with rheometer A equipped using a plate with diameter d = 25 mm and roughness R_q = 2 - 4 μm. Use the settings determined in the amplitude sweep experiments (2.1). The required paste volume is 0.49 mL.
      1. Carry out the three-stage oscillation test with different oscillation amplitudes at constant frequency (f = 1 Hz).
         NOTE:
         Stage I: Small oscillation amplitude within the LVE is applied for a period of 300 s to obtain the shear moduli of the initial state. For paste B $\hat{\gamma}_I$ = 0.025%.
         Stage II: The large strain amplitude ($\hat{\gamma}_{II}$ = 80%) determined in step 2.1 is applied in the oscillatory shear mode for t_{II} = 50 s, 150 s or 600 s for time dependence investigations. For deformation dependence investigations the strain amplitudes between $\hat{\gamma}_{II}$ = 0.025% and $\hat{\gamma}_{II}$ = 100% are applied each for constant time (t_{II} = 150 s).
         Stage III: The same small oscillation amplitude like in stage I is applied for 1,200 s to follow the recovery over a longer period of time.
      2. Repeat steps 1.2.1.3 - 1.2.1.8 to complete three stage oscillation tests three times. Clean the measuring gap with ethanol before each measurement.
      3. Plot the moduli G' and G" versus time in a semi-log plot (see **Figure 14** and **Figure 15 (a)**).

3. Stretching Behavior Determination — a Snap-off Simulation

1. Stretching behavior measurements with the capillary breakup elongational rheometer
   1. Perform stretching experiments with the capillary breakup elongational rheometer. Use two cylindrical pistons with a diameter d = 6 mm. Stretch the pastes at varying velocities from the initial gap height h = 1 mm till the filament breaks.
      NOTE: Please note that this is not a typical filament thinning experiment controlled by surface tension. This test can also be done with a screen mesh attached with the emulsion side on the upper piston and a wafer substrate on the bottom. This way printing process during metallization of mono- and multicrystalline industrially pre-processed Si-wafer is mimicked.
      1. Adjust the measuring settings for stretching experiments. Vary the stretching velocities (*e.g.*: 7.5 mm s^{-1}, 11 mm s^{-1} and 110 mm s^{-1}) to see the change in filament deformation and breakup behavior.
      2. Turn on the high speed camera to record the change in filament shape. Set the frame rate to minimum 250 fps and turn on the backlight to trace the filament deformation. Also adjust the high speed camera settings, especially the image sharpness, the contrast and brightness of the exposure field.
      3. Before filling the measuring gap with silver paste, mix the sample in its reservoir to ensure the paste is homogeneously blended. After mixing, fill up the measuring gap with paste.
      4. Take a small amount (28.3 μL) of the blended paste to apply it on the bottom piston. Bring the upper piston to the measuring position (measuring gap height h = 1 mm) and clean up the excess sample from the edge of the geometry.
      5. Start the measuring device and the recordings of the filament deformation at the same time.
      6. Repeat the measurement three times. For each measurement, clean the measuring gap with ethanol and repeat steps 3.1.1.3 - 3.1.1.5.
      7. Choose the first picture showing filament breakage to evaluate the piston position x_{break} at which the filament breaks. Calculate the critical stretch ratio $(x_{br} - x_0) / x_0 = \Delta x_{br} / x_0$. Determine this quantity for different stretching velocities (**Figure 16**).

2. Stretching force measurement with the tensile tester
   1. For tensile tester experiments use a piston with a diameter d = 5 mm. Record the resulting tensile force during stretching.
      1. Adjust the measuring settings for stretching experiments. Vary the stretching velocities, *e.g.* v = 10 mm s^{-1}, 20 mm s^{-1}, 30 mm s^{-1}, and 40 mm s^{-1} and measure the change in stretching force with a 50 N load cell. Set the initial gap height h to h = 1 mm and the end position to h_{end} = 12 mm.
      2. Before filling the measuring gap with silver paste, mix the sample in its reservoir to ensure the paste is homogeneously blended.

3. Apply the paste to the bottom plate of the tensile tester. Bring the upper plate to the measuring position and clean up the excess sample from the edge of the geometry.
4. Start the measuring device and the recordings of the filament elongation at the same time.
5. Repeat the measurement three times. For each measurement clean the measuring gap and repeat steps 3.2.1.2 - 3.2.1.4.
6. From the F vs. Δx data the maximum force F_{max} detected during extension and the stretch ratio at break $\Delta x_{br} / x_0$ are obtained as shown in **Figure 17 (a)**. Plot $\Delta x_{br} / x_0$ vs. the different stretching velocities (**Figure 17 (a)**). Plot F_{max} vs. stretching velocity (**Figure 17 (b)**).

Representative Results

The viscosity is a key parameter in fluid processing and for multiphase fluids its dependence on shear rate is often determined using parallel-plate rotational rheometry. For highly concentrated suspensions this is neither a straight forward nor a trivial task and the definition of a suitable measuring protocol can be challenging. Here it is demonstrated how highly concentrated silver pastes can be rheologically characterized combining rotational rheometry and video recordings. A robust experimental protocol for determination of the steady shear viscosity is established and the accessible shear rate range is determined. **Figure 1** represents an overview of apparent viscosity and apparent shear stress vs. the applied apparent shear stress for paste B. The measurement is done with a plate roughness of $R_q = 2 - 4$ µm. Cutouts from video recordings permit the division of the obtained flow curve into three sections. In section one wall slip dominates. The upper plate glides without paste deformation. In this section the shear stress is constant. Paste deformation sets in at $\dot\gamma_{min, app} = 0.07$ s^{-1} marking the onset of section two. At the same time the shear stress begins to increase. The deformation of the paste and the stress increase monotonically until section three is reached. At a critical shear rate or angular speed the paste creeps out of the gap and at the same time apparent viscosity and shear stress drop strongly due to the sample spill. Accordingly, the viscosity and shear stress curves exhibit a characteristic kink which occurs at about $\dot\gamma_{max, app} = 2.5$ s^{-1}. This $\dot\gamma_{max, app}$ marks the onset of sample spill. The higher the shear rate the faster the paste is ejected. The viscosity of the paste is accessible only in the shear rate range at $\dot\gamma_{min, app} < \dot\gamma_{app} < \dot\gamma_{max, app}$. However, since the deformation inside the gap is not known and *a priori* must not be the same as observed at the rim the viscosity data even in that nominal shear rate range has to be treated as the apparent values. The shear stress τ_{app} at the rim of the plate r_{max} is calculated from the applied torque T in the following way $\tau_{app} = T (2\pi r_{max}^3)^{-1} [3 + d(\ln T) / d(\ln \dot\gamma_{app})]$. The apparent shear rate $\dot\gamma_{app}$ at the edge of the plate is calculated from the angular velocity Ω of the plate and the gap height h according to $\dot\gamma_{app} = \Omega (r_{max} / h)$[34]. Since the true deformation and stresses inside the gap are not known these calculated stress and shear rate values have to be treated as apparent or nominal values.

In soft matter often a critical stress, the so-called apparent yield stress $\tau_{y, app}$, is found at which a transition from an elastic reversible deformation to irreversible flow is observed. This yield stress is a key factor in paste formulation regarding classical screen-printing as well as emerging additive manufacturing techniques. A high yield stress is desirable to ensure shape accuracy after printing. Generally, the yield stress is determined from the kink in the deformation vs. shear stress curve using the tangent intersection method as exemplarily shown in **Figure 2**. Often this is done using a so-called vane geometry guaranteeing reliable and significant results without the effect of slip[35,36]. Measuring the yield stress with the parallel-plate geometry is another option which has to be carefully validated. Wall slip or shear banding phenomena often observed in highly filled suspensions may interfere with the yield stress evaluation. Therefore, the effect of plate roughness on $\tau_{y, app}$ determination is investigated. Results for the yield stress values obtained for paste A and B in stress sweep experiments at different plate roughness are shown in **Figure 3**. Increasing the plate roughness causes an increase in calculated yield stress, whereas the variation in gap height h does not affect determination of this quantity. **Figure 4** displays cutouts of the video taken for paste A at a plate roughness of $R_q = 1.15$ µm and a gap height of h = 1 mm. Soot particles were placed on the sample rim as a marker and endoscopic video imaging was used to characterize the deformation at the sample rim. The paste glides on the bottom plate at stresses up to $\tau_{app} = 600$ Pa while it sticks to the upper plate. A plug flow is formed in the measuring gap, *i.e.* the sample is not deformed and the determination of a yield stress or viscosity is pointless even though a kink in the corresponding apparent deformation vs. shear stress curve seems to imply a transition from elastic deformation to viscous flow. Similar behavior is obtained for other gap heights for paste A as well as paste B. So a plate roughness of $R_q = 1.15$ µm is not appropriate for the determination of yield stress or viscosity of such highly filled silver pastes. In contrast, for a plate roughness $R_q = 2 - 4$ µm (as declared by the manufacturer) video imaging confirms the formation of a shear deformation profile at the rim (**Figure 5**) as necessary for a reliable and well-defined rheological measurement. Plug flow is avoided and for paste A uniform flow sets in at $\tau_{app} = 1,360$ Pa. Similar flow behavior was observed for paste B. So this choice of plate roughness allows for a reliable yield stress measurement. Choosing a higher plate roughness $R_q = 9$ µm results in higher yield stress values than obtained for plate roughness $R_q = 1.15$ µm and $R_q = 2 - 4$ µm. This effect is much more pronounced for paste A than for paste B. The video recordings show that no shear profile is formed with paste A during this measurement (**Figure 6**). At a stress $\tau_{app} = 1,880$ Pa the upper plate starts moving without paste deformation. A stress of $\tau_{app} = 2,605$ Pa causes gliding of the paste on the bottom plate still without paste deformation. The critical stress corresponding to the kink in the deformation vs. stress curve does not mark the transition from elastic to viscous deformation, *i.e.* it is not the apparent yield stress. Instead it marks the onset of slip and plug flow and has to be considered as critical slip stress τ_{slip}. In contrast, no plug flow was observed for paste B using the $R_q = 9$ µm plate (**Figure 7**). The deformation of the paste starts at $\tau_{app} = 1,430$ Pa and is fully developed at $\tau_{app} = 1,597$ Pa. At higher shear stress ($\tau_{app} = 1,880$ Pa) shear banding occurs, *i.e.* only an intermediate narrow layer of the sample is sheared. The yield stress obtained from the deformation vs. stress data with the $R_q = 9$ µm plate is close to that obtained with $R_q = 2 - 4$ µm in case of paste B, but it is pointless to use this rough plate for $\tau_{y, app}$ determination of paste A. To double-check the parallel-plate $R_q = 2 - 4$ µm results, the yield stress was also measured with the vane geometry. This geometry is inherently not affected by wall slip effects and the onset of rapid vane rotation at a certain applied stress is unequivocally related to the structural breakdown within the paste in the cylindrical plane defined by the diameter of the vane[35,36]. **Figure 8** shows that the results obtained using the vane geometry agree very well with those obtained from parallel-plate rheometry with $R_q = 2 - 4$ µm. Based on the findings presented above, all further experiments were performed using a plate with roughness $R_q = 2 - 4$ µm except for the wall slip velocity measurements. The plates with roughness $R_q = 1.15$ µm and $R_q = 9$ µm cannot be recommended for yield stress and viscosity determination of silver pastes or other highly filled suspensions similar to those investigated here. Finally, it is stated that the yield stress of paste A is higher than that of paste B.

Wall slip is another important parameter for successful printing. The higher the wall slip, the better the paste flows through the screen mesh openings[32]. The wall slip velocity, *i.e.* the relative velocity of the moving plate and the adjacent paste layer, can be evaluated directly from video recordings irrespective of plug flow or shear deformation prevailing in the gap. A smooth upper plate and a rough bottom plate have to be used when performing these experiments[25,27,28,30]. If the sample within the gap is at rest, the slip velocity is directly given by the speed of the upper plate. **Figure 9** displays the wall slip velocity vs. shear stress as determined under this latter conditions using a plate with $R_q = 1.15$ µm. Slip clearly occurs at stresses far below the yield stress similar as observed for concentrated emulsions and pastes of soft microgel particles[28,29,30]. For paste A, higher wall slip velocities are obtained than for paste B irrespective of applied stress. In both cases, slip velocity increases linearly with applied stress. However, the obtained slope $m_A = 0.33$ µm (Pa s)$^{-1}$ for paste A is nearly three times higher than the slope $m_B = 0.12$ µm (Pa s)$^{-1}$ obtained for paste B. Similar as observed previously[28,29,30], a characteristic slip velocity V* at about a stress level corresponding to the yield stress is found and above τ_y slip is hardly measurable. For paste A and B, $V_A^* = 0.37$ mm s^{-1} and $V_B^* = 0.11$ mm s^{-1}, respectively.

The sample spillover is attributed to the strong centrifugal force acting on the high density micron-sized particles and should therefore be controlled by the angular or rotational speed n_{crit} at which the centrifugal force dominates over viscous friction. To test this, the measuring gap height h was increased from 0.2 mm to 2 mm. The intensity of sample spillover increases with gap height h and shear rate. The wider the gap height the earlier sample spill sets in, *i.e.* $\dot{\gamma}_{crit}$ is lower (**Figure 10**). **Figure 11** demonstrates that sample spill sets in at a critical angular speed n_{crit} irrespective of sample height h between 0.5 mm and 2 mm. For paste A, the critical rotational speed is $n_{crit, A} \approx 0.6$ min^{-1} and for paste B it is $n_{crit, B} \approx 1.7$ min^{-1}. The finding $n_{crit, A} < n_{crit, B}$ might be due to different vehicle viscosity or due to varying silver particle size. However, both pastes exhibit much higher n_{crit} values for a measuring gap height h = 0.2 mm. Thus, decreasing the gap height allows for a wider shear rate range in which viscosity determination is possible. The reason for the high n_{crit} values found for h = 0.2 mm is not yet clear. This might be due to a stronger contribution of surface tension at the sample rim or due to the formation of aggregates clogging the narrow gap. Further investigations are necessary to clarify that. **Figure 10** further confirms that for $\dot{\gamma}_{app} = 0.07$ s^{-1} - 2.5 s^{-1} the apparent viscosity data obtained at different gap heights do not vary systematically, *i.e.* wall slip is negligible under these experimental conditions. Varying the shear rate from high to low or from low to high values yields the same viscosity data as long as n_{crit} is not exceeded, *i.e.* no spillage takes place, *i.e.* there is no evidence of irreversible structural change within the sample.

A capillary rheometer is used to determine the paste viscosity especially at process-oriented high shear rates. The Weissenberg-Rabinowitsch correction for non-parabolic velocity profile is done here to get the true shear rate in the case of non-Newtonian fluids[34]. The entrance pressure loss is negligible because of the high L/d ratio >> 1, but the occurrence of wall slip has not been investigated in this case and therefore data have to be treated as apparent viscosity values. **Figure 12** displays the apparent viscosity for both pastes A and B determined with parallel-plate rotational rheometry and capillary rheometry. Remarkably, the data obtained from both experimental techniques seem to agree very well for both pastes suggesting that wall slip is of minor relevance in the capillary rheometry measurements performed here. Finally, paste A and B exhibit similar apparent viscosity at low shear rates but viscosity of paste A is higher than that of paste B in the high shear regime.

Steady shear measurements using parallel-plate rotational rheometers have to be performed carefully and may be disturbed by wall slip, shear banding or sample spillage as extensively discussed above. Therefore, using oscillatory shear experiments have been suggested to characterize structural breakdown and recovery of silver pastes during the screen-printing process. This is done in a three stage oscillatory test as suggested by Hoornstra, Zhou and Thibert[10,15,21]. First, an amplitude sweep has to be performed to determine the linear and non-linear response regime at a pre-selected frequency (**Figure 13**). The linear viscoelastic regime distinguishes itself by constant, γ-independent modulus values and G' > G''. The decay of the storage modulus G' at large γ is chosen as a criterion to identify the onset of the non-linear response regime. The characteristic deformation amplitude γ_c marking the transition from linear to non-linear response is defined as the amplitude at which G' has decreased to 80% of its average initial value G'_0 in the linear regime: $G'(\gamma_c) = 0.8\ G'_0$. In stage I and III of the test, a small oscillation amplitude within the linear viscoelastic response regime, *i.e.* $\gamma < \gamma_c$ is selected to characterize the rest structure of the paste (stage I) as well as the time dependence and degree of recovery in stage III of the test after the destruction of the initial structure due to a high deformation amplitude applied in stage II. **Figure 14** shows corresponding results for paste B. In stage I, the paste is deformed at $\gamma = 0.025\%$ and G' is higher than G'', *i.e.* the elastic behavior of the paste is predominant. When deformation is increased in stage II, G'' is higher than G' ensuring the structural breakdown within the paste during this period of large deformation. Stage III simulates the resting of the finger lines on the substrate after printing. In this stage G' is higher than G'' again, but G' and also G'' are both lower than the respective initial G' and G'' values before the paste structure was destroyed. The video recordings confirm that this is not related to the effects like wall slip, plug flow or sample spill. The paste deforms uniformly during oscillatory shear, sticks to the plate, and indicates neither wall slip nor sample spill. Therefore, it can be concluded that the incomplete recovery of the shear moduli indicates an irreversible structural change within the sample due to the applied large amplitude shear in stage II. The data shown in **Figure 15 (a)** reveal that the degree of irreversible structural change does not depend on the duration of the large deformation amplitude oscillatory shear applied in stage II. The results in stage III do not vary for different periods of shearing time t_{II}. However, the value of the selected deformation amplitude in stage II has a strong impact on the degree of structural recovery. This is obvious from **Figure 15 (b)** showing the difference between the storage modulus values determined in stage III and I ΔG' normalized by the initial modulus value G'_I. For $\gamma > 20\%$, *i.e.* at deformations corresponding to the crossover of G' and G'' (see **Figure 13**) paste B recovers only 30% of its initial value and paste A only 10%. This is considered a paste property crucial for various coating operations and its dependence on paste composition will be addressed in future work. Note, the structural recovery immediately after cessation of large amplitude oscillatory shear in stage II would be of utmost relevance especially for the screen-printing process but the commercial rheometer used here does not allow for determination of reliable data within the first second after changing γ.

Filament stretching experiments have been performed to simulate the snap-off during screen-printing. The snap-off belongs to the final step of screen-printing. **Figure 16** demonstrates that the filament lengths at break increases with increasing stretching velocity for both pastes. Breakage always occurs at lower stretch ratio $(x_{br} - x_0) / x_0 = \Delta x_{br} / x_0$ for paste B than for paste A, but this difference seems to decrease slightly with increasing stretching velocity. Since the filament breakage of paste B happens at a lower stretch ratio this paste may have better snap-off properties.

The results obtained with the capillary breakup elongational rheometer imaging setup are confirmed by the tensile tester experiments. Corresponding results are shown in **Figure 17**. Again the stretch ratio at which the filaments break increase with increasing stretching velocity (**Figure 17 (a)**) and paste B breaks at lower $\Delta x_{br} / x_0$ values than paste A. However, the absolute values $\Delta x_{br} / x_0$ obtained with the capillary breakup elongational rheometer are always higher than corresponding values obtained with the tensile tester. This is attributed to the different plate diameters d = 6 mm and d = 5 mm, *i.e.* different initial sample volumes for the capillary breakup elongational rheometer and tensile tester. Finally the tensile tester also provides a second characteristic parameter the maximum force F_{max} acting on the filament during stretching. This quantity also increases linearly with increasing separation speed but in this case the values obtained for paste B are larger than those for paste A. Further investigations will be needed to disclose the relevance of F_{max} for the screen-printing process or other coating operations.
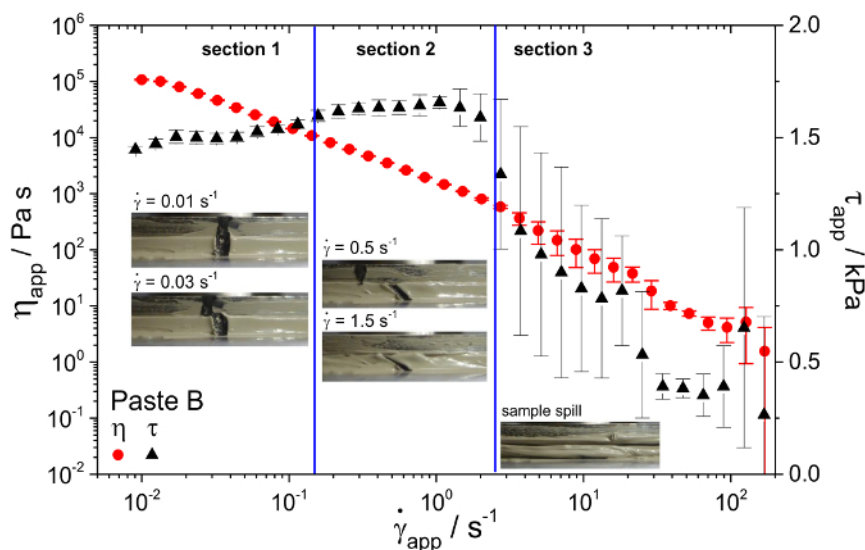
Figure 1. Apparent viscosity in controlled shear rate parallel-plate rotational rheometry. Overview of the resulting apparent viscosity and shear stress measured in controlled shear rate mode with a parallel-plate rheometer (short: PP), plate roughness R_q = 2 - 4 µm and gap height h = 1 mm. Classification of apparent shear rate in three sections based on video recordings during measurement. Wall slip, paste deformation and sample spill are highlighted in the video recording cutouts. Paste B is chosen exemplarily here, but similar results were obtained for paste A. The error bars are calculated as the standard deviation obtained from at least three independent measurements. Please click here to view a larger version of this figure.

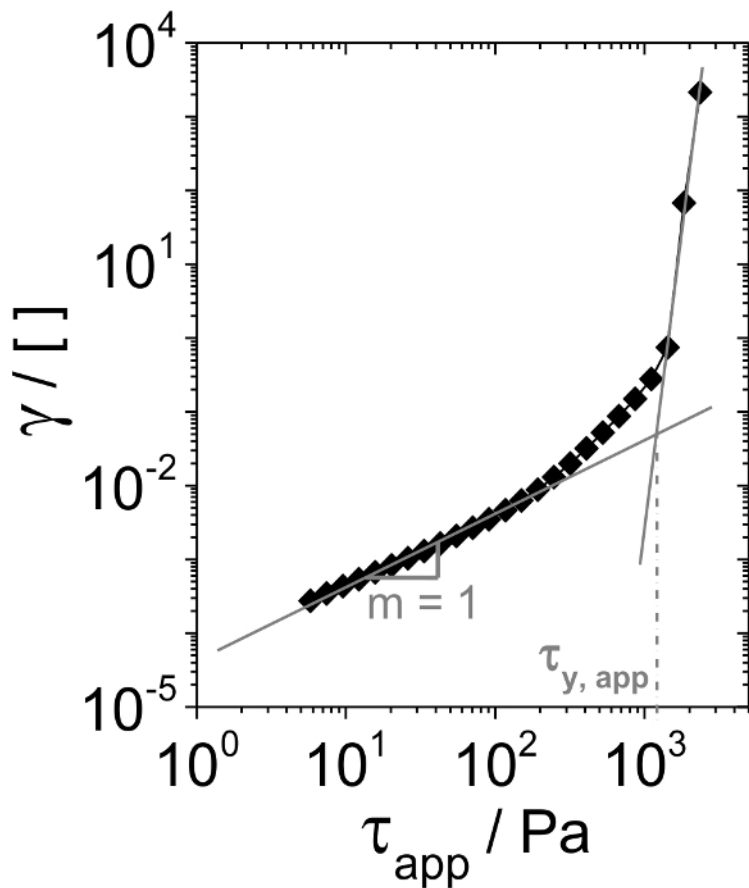**Figure 2. Applying the tangent intersection point method for yield stress determination.** The deformation γ, *i.e.* the displacement of the upper plate divided by the gap height, is plotted versus the applied nominal shear stress τ_{app}. The shear stress controlled measurement is done with a plate roughness $R_q = 2 - 4 \ \mu m$ and a gap height $h = 1$ mm. Paste B is chosen exemplarily here, but similar results were obtained for paste A. Please click here to view a larger version of this figure.
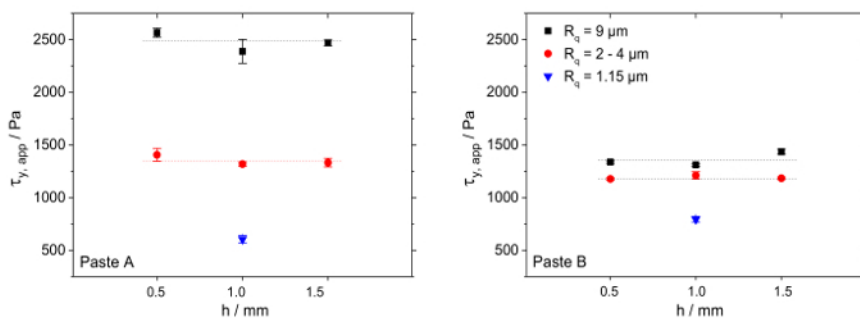
Figure 3. Effect of plate roughness on apparent yield stress. The resulting apparent yield stress for different plate roughness $R_q = 1.15 \ \mu m$, $R_q = 2 - 4 \ \mu m$ and $R_q = 9 \ \mu m$ vs. gap height h. Results depend on the plate roughness R_q and is independent of varying the measuring gap height (left: paste A, right: paste B). The error bars are calculated as the standard deviation obtained from at least three independent measurements. Please click here to view a larger version of this figure.
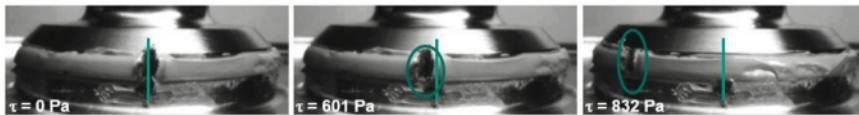
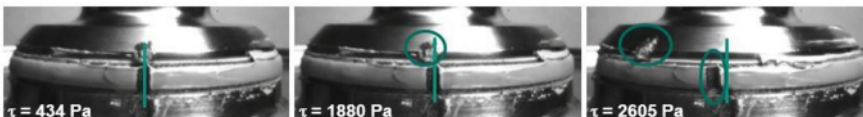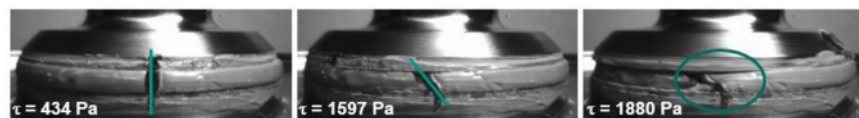**Figure 4. Cutouts from video recordings at varying shear stress.** Here using the example of paste A measured with plate roughness R_q = 1.15 µm. Please click here to view a larger version of this figure.


Figure 5. Cutouts from video recordings at varying shear stress. Here using the example of paste A measured with plate roughness R_q = 2 - 4 µm. Please click here to view a larger version of this figure.

Figure 6. Cutouts from video recordings at varying shear stress. Here using the example of paste A measured with plate roughness R_q = 9 µm. Please click here to view a larger version of this figure.

Figure 7. Cutouts from video recordings at varying shear stress. Here using the example of paste B measured with plate roughness R_q = 9 µm. Please click here to view a larger version of this figure.
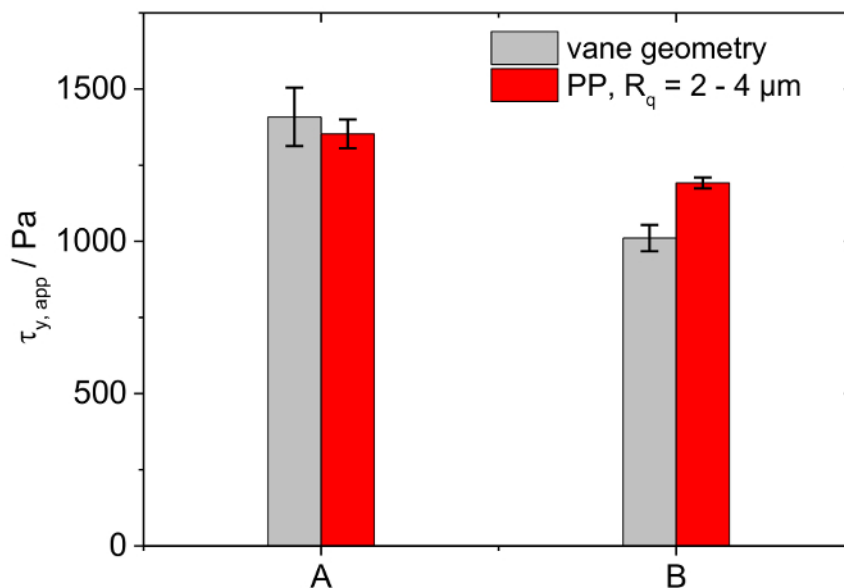
Figure 8. Resulting yield stress. A comparison of the yield stress for paste A and B determined with the vane geometry and the R_q = 2 - 4 µm parallel-plate geometry. The error bars are calculated as the standard deviation obtained from at least three independent measurements. Please click here to view a larger version of this figure.
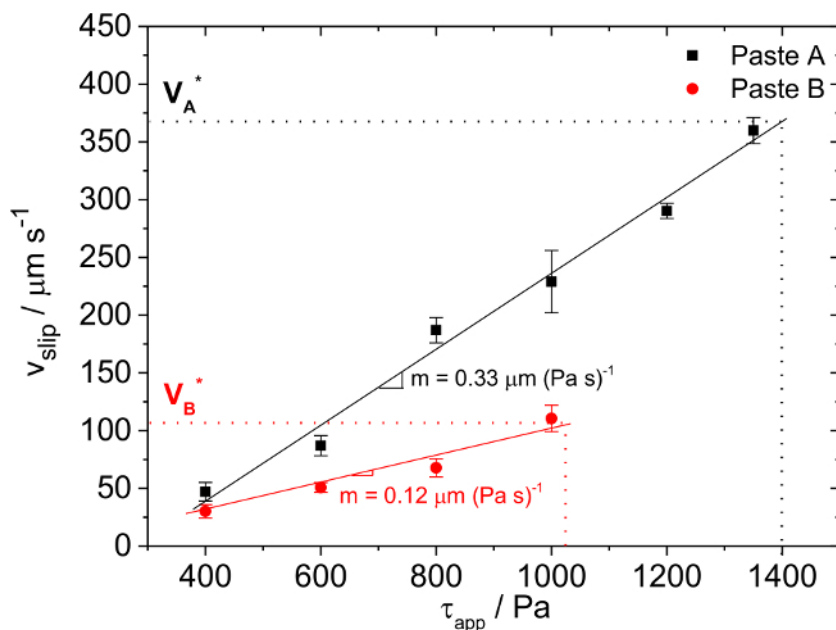
**Figure 9. Dependence of wall slip on shear stress.** Wall slip velocity v_{slip} vs. shear stress τ for paste A and B determined with $R_q = 1.15$ µm parallel-plate geometry at gap height $h = 1$ mm. The characteristic wall slip velocity obtained at the yield stress of the material is indicated as V*. The error bars are calculated as the standard deviation obtained from at least three independent measurements. Please click here to view a larger version of this figure.
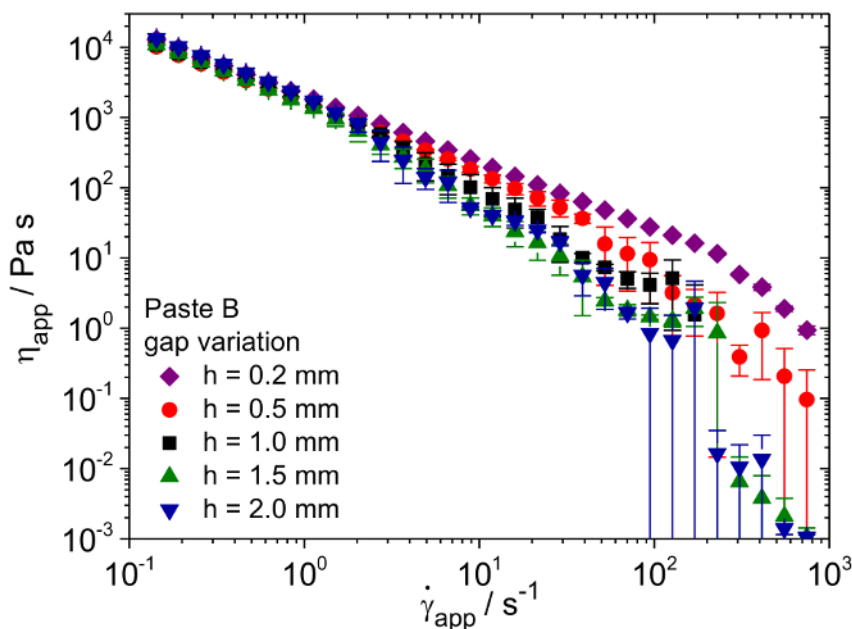
Figure 10. Effect of gap height on sample spill. Apparent viscosity at varying measuring gap height h in controlled shear rate mode for paste B and plate roughness $R_q = 2 - 4$ µm. The gap height is varied between $h = 0.2$ mm and $h = 2.0$ mm. Downward kink of viscosity curve sets in at higher shear rates when a lower gap height is chosen. The gap height is varied between $h = 0.2$ mm and $h = 2.0$ mm. The error bars are calculated as the standard deviation obtained from at least three independent measurements. Please click here to view a larger version of this figure.

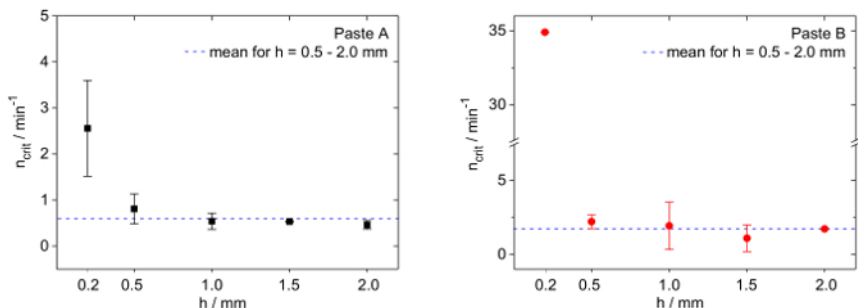**Figure 11. The critical rotational speed at which sample spill sets in.** Rotational speed n_{crit} at which the downward kink of the viscosity curve sets in vs. gap height h using parallel-plate geometry with R_q = 2 - 4 μm (left: paste A, right: paste B). Sample spillover sets in at this characteristic rotational speed as confirmed by video recordings. For paste A sample spill sets in at $n_{crit, A}$ = 0.6 min^{-1} and for paste B at $n_{crit, B}$ = 1.7 min^{-1} for gap height h ≥ 0.5 mm. The error bars are calculated as the standard deviation obtained from at least three independent measurements. Please click here to view a larger version of this figure.
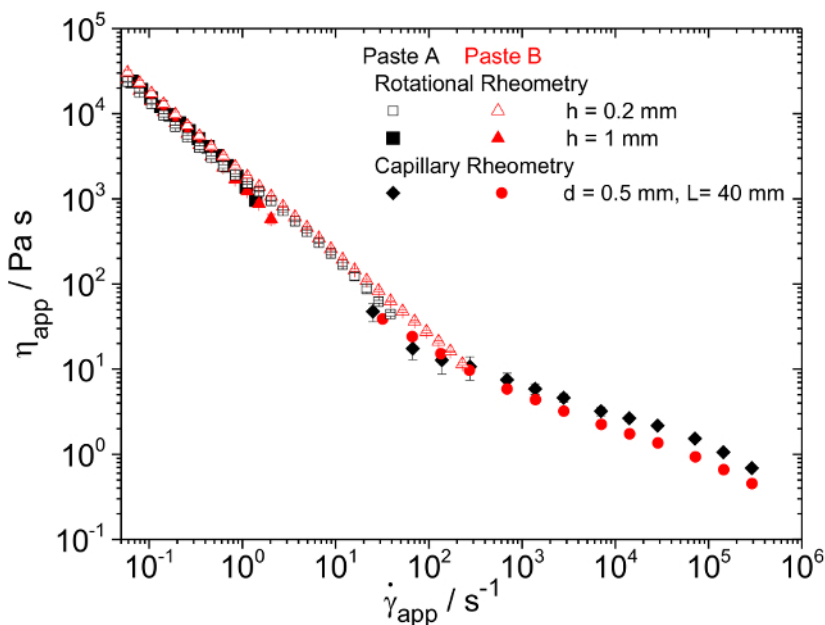

Figure 12. Viscosity in a wide shear rate range. Apparent viscosity of paste A and B determined in a wide shear rate range using parallel-plate rotational rheometry (gap height h = 0.2 mm and h = 1 mm; R_q = 2 - 4 μm) and capillary rheometry (d = 0.5 mm and L = 40 mm). The error bars are calculated as the standard deviation obtained from at least three independent measurements. Please click here to view a larger version of this figure.

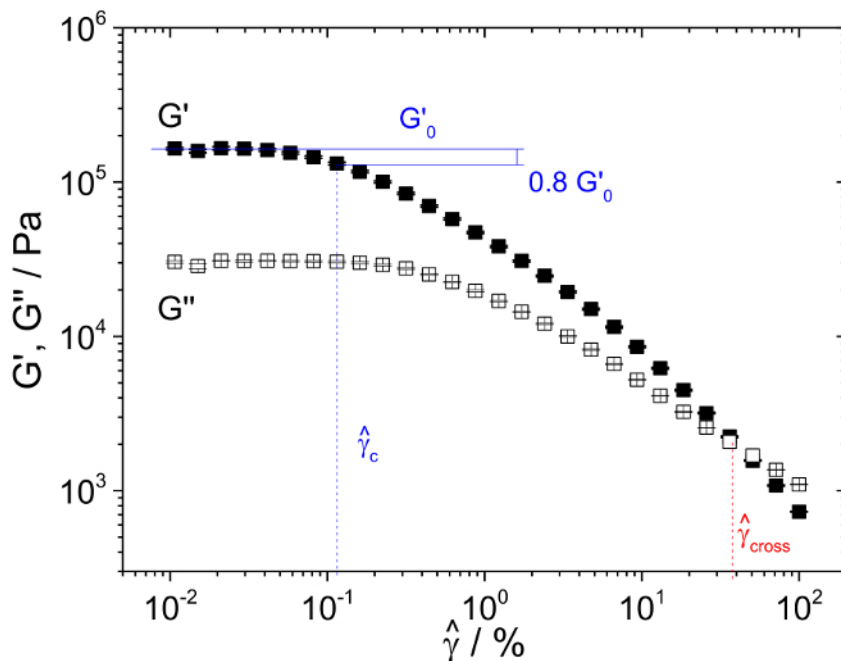April 2017 | 122 | e55377 | Page 12 of 17

Figure 13. Determination of the linear and non-linear response regime in oscillatory shear. Amplitude sweep test for paste B: G', G'' vs. deformation amplitude $\hat{\gamma}$ at fixed frequency f = 1 Hz. Test performed using a rotational rheometer equipped with parallel-plate geometry (R_q = 2 - 4 μm, gap height h = 1 mm). The error bars are calculated as the standard deviation obtained from at least three independent measurements. Please click here to view a larger version of this figure.
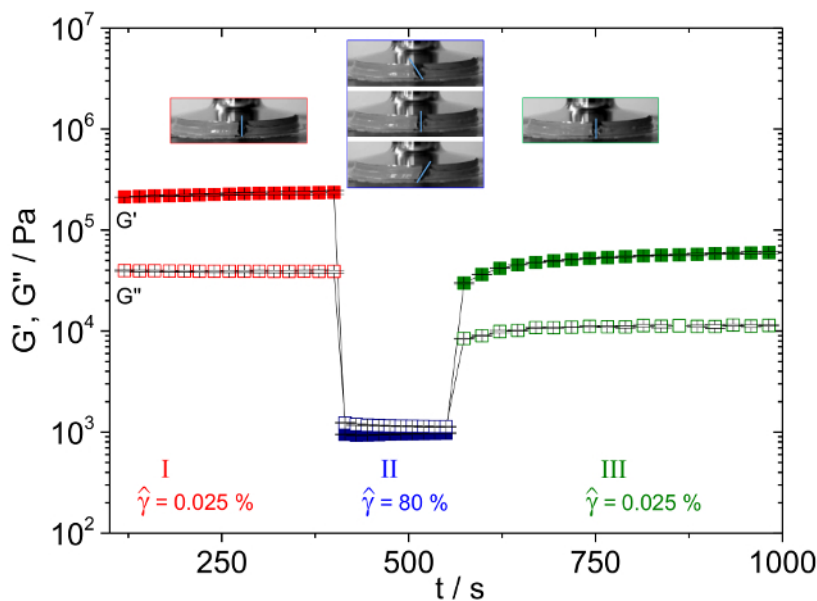

Figure 14. Three stage structural recovery test. Three stage structural recovery test for paste B performed at constant frequency f = 1 Hz with a parallel-plate rotational rheometer (plate roughness R_q = 2 - 4 μm). The applied deformation amplitude $\hat{\gamma}$ in stage I is 0.025%, in stage II $\hat{\gamma}$ = 80% and in stage III $\hat{\gamma}$ = 0.025%. Video recordings confirm homogeneous sample deformation throughout the gap, no wall slip, shear banding, plug flow or sample spillage occurs. The error bars are calculated as the standard deviation obtained from at least three independent measurements. Please click here to view a larger version of this figure.
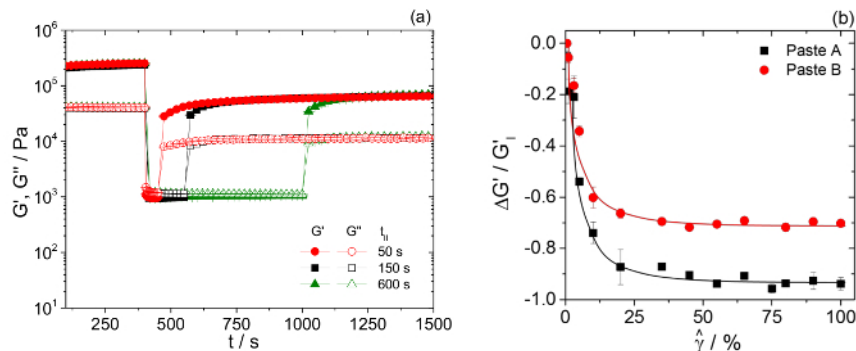
Figure 15. Structural recovery tests. (**a**) Effect of shearing time on structural recovery. Structural recovery of paste B for $\hat{\gamma}_{II}$ = 80% and different duration of stage II, t_{II} = 50 s, 150 s and 600 s. (**b**) Effect of deformation amplitude on structural recovery. Relative irreversible structural change (G'(t → ∞) - G'(t = 0)) / G' (t = 0) = ΔG' / G'$_I$ as a function of deformation amplitude $\hat{\gamma}$ applied in stage II of the three stage structural recovery test determined for paste A and B at constant t_{II} = 150 s. The error bars are calculated as the standard deviation obtained from at least three independent measurements. Please click here to view a larger version of this figure.
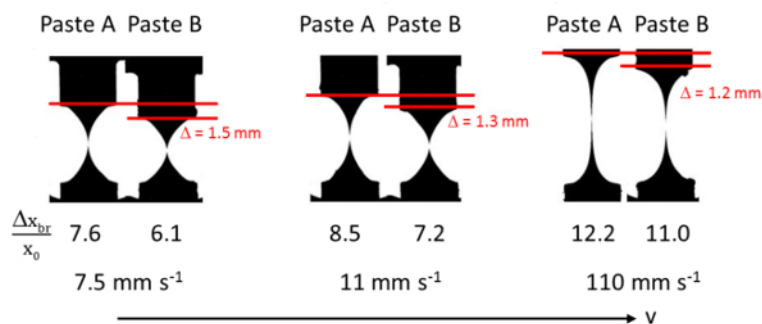

Figure 16. Optical determination of filament breakage in elongational deformation. Critical tensile stretch ratio at which filament breakage occurs for pastes A and B at different stretching velocities as obtained using the capillary breakup elongational rheometer (initial gap height h = 1 mm). Please click here to view a larger version of this figure.
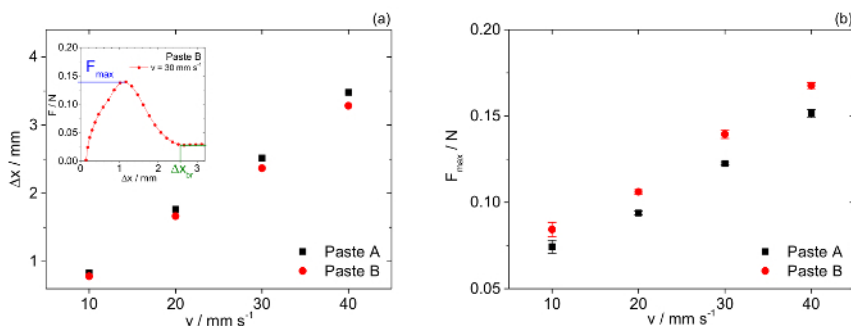

Figure 17. Tensile testing — axial force during elongational deformation. Resulting Δx_{br} / x_0 (**a**) and resulting force F_{max} (**b**) vs. stretching velocity obtained for paste A and B with the tensile tester. The initial gap height is h = 1 mm and the piston diameter d = 5 mm. The insert displays raw force F vs. stretch ratio data for paste B obtained at v = 30 mm s^{-1} to demonstrate the determination of F_{max} and Δx_{br}. The error bars are calculated as the standard deviation obtained from at least three independent measurements. Please click here to view a larger version of this figure.

Methods	Information	Paste characteristics	Plate roughness R_q
steady shear	apparent viscosity $\eta_{apparent}$	Paste A > Paste B	2 – 4 µm
	yield stress τ_y	Paste A > Paste B	2 – 4 µm; vane geometry
	wall slip behavior v_{slip}, V^*	Paste A > Paste B	1.15 µm
	critical rotational speed n_{crit}	Paste A > Paste B	2 – 4 µm
oscillatory shear	elastic modulus G_0	Paste A > Paste B	2 – 4 µm
	three stage structural recovery (testing time and deformation dependency)	Paste A < Paste B	2 – 4 µm
stretching behavior determination	elongation at filament breakage	Paste A > Paste B	-
	maximal tensile force during elongation	Paste A < Paste B	-

Table 1. Overview of applied methods, corresponding characteristic information and differences between specific flow properties of paste A and B. Please click here to view a larger version of this table.

Discussion

A comprehensive rheological characterization of highly concentrated suspensions or pastes is mandatory for a targeted product development meeting the manifold requirements during processing and application of such complex fluids. This investigation includes the determination of yield stress, viscosity, wall slip velocity, structural recovery after large deformation and elongation at break as well as tensile force during filament stretching. A summary of all applied methods, obtained information, and paste characteristics are summarized in **Table 1**.

The importance of video recordings for reliable determination of rheological quantities of highly filled suspensions showing wall slip, shear banding and sample spillover in parallel-plate rotational rheometry is demonstrated. Video recordings enable the determination of the true deformation profile and the flow field at the sample rim using appropriate markers. It is necessary to study this deformation behavior before analyzing the results of rheological experiments. Thus measurement parameter settings and plate roughness values can be identified for which viscosity measurements are possible. The paste yield stress can be determined either using a vane geometry or plate-plate geometry with appropriate roughness.

Viscosity determination is possible using plate-plate geometry only with a carefully selected plate roughness depending on sample composition. Higher roughness does not necessarily result in lower wall slip. The shear rate or shear stress range in which viscosity determination can be done is limited by the yield stress and the onset of sample spill.

Furthermore, the slip velocity can be measured directly and measuring conditions at which plug flow, shear banding or sample spillover occur can be identified clearly. For wall slip measurements smooth surfaces were used as the upper shearing plate and a rough bottom plate to allow slip only at the upper plate. This slip velocity can be calculated directly from the angular velocity of the upper plate. For both pastes slip occurs at stress levels well below the apparent yield stress. Similar observations have been reported for suspensions of glass beads[25], clay suspensions[27], soft microgel pastes as well as for emulsions[28,29,30]. Here a linear increase of v_{slip} with τ_{app} is found. This is in line with the observations of Aral *et al.*[25] who also determined v_{slip} using visualization of the flow field at the rim of the investigated glass bead suspensions.

Seth *et al.* have shown that the scaling of slip velocity with applied stress is controlled by the interaction between the soft particles they used in their study and the wall. For the case where there is no specific adherence of particles to the wall, they also find a linear relationship between v_{slip} and stress but a quadratic scaling is found for the particles weakly adhering to the wall[28,29,30]. The studies on soft particle pastes also reveal a characteristic slip velocity V^* at the yield stress and a elastohydrodynamic model is presented[29] allowing to calculate V^* from physical fluid and particle parameters which can be determined independently: $V^* \sim \gamma_y^2 (G_0 R / \eta_s) (G_P / G_0)^{1/3}$. This characteristic slip velocity depends on the pastes yield strain γ_y and elastic modulus G_0, solvent viscosity η_s, as well as particle radius R and modulus G_P. The values resulting from this simple estimate ($V_A^* = 375$ µm s^{-1} and $V_B^* = 118$ µm s^{-1}) agree very well with the experimental results (**Figure 9**) not only with respect to the order of magnitude but also regarding the difference between paste A and B.

Sample spillage is observed here at a critical rotational speed characteristic for each paste. Spillage does not occur in the pure vehicles. This phenomenon limits rheological characterization of the pastes and may also be relevant for certain processing or coating operations but its physical origin still remains unsolved.

Video recordings further indicate that wall slip, plug flow and sample spill can be excluded during oscillatory shear tests. Therefore, the decrease and increase in shear moduli observed during three stage oscillatory shear tests with small oscillation amplitude in stage I and III as well as large deformation amplitude $\gamma > \gamma_c$ can be directly attributed to structural break down and recovery. It could be shown that the degree of irreversible structural change during oscillatory shear increases with increasing deformation amplitude in stage II until a saturation is reached at deformations corresponding to the crossover of G' and G'' in the amplitude sweep test, but the irreversible damage is independent of the duration of high amplitude shear in stage II. The change in modulus and hence sample structure due to large shear deformation in stage II is termed irreversible here since after waiting times of more than 10^4 s, the storage modulus is far lower than its initial value (data not shown). The data shown in **Figure 15** are restricted to waiting times of 1,500 s for the sake of clearness. However, it should be noted that the time scale of the printing process is on the order of seconds or even below. This is not accessible with the conventional rotational rheometer setup used in this study.

The gap heights used in this study are also much larger than typical mesh openings in screen-printing of modern printed electronics. Rheological measurements using plate-plate geometry cannot be done at such small gap openings due to limitations of mechanical adjustment for large plates typically used in rheological measurements. Furthermore, large gap separations have been chosen here to ease visualization of the sample deformation at the rim.

Filament stretching tests using a capillary breakup elongational rheometer and a tensile tester can be used to characterize the deformation and breakup behavior of highly filled pastes in elongational flows. The elongation at the break and the maximum force during elongation are parameters obtained from these tests and may be related to the squeegee snap-off during screen-printing.

Finally, significant differences were observed in all the experiments described above for the two commercial silver pastes investigated in this study. An extended discussion of the relevance of the rheological paste properties for their performance will be addressed in a subsequent paper based on data for a broad variety of different pastes and vehicles.

Disclosures

The authors have nothing to disclose.

Acknowledgements

References

1. Mathews, N., Lam, Y. M., Mhaisalkar, S. G., & Grimsdale, A. C. Printing materials for electronic devices. *Int. J. Mater. Res.* **101,** 236-250 (2010).
2. Ralph, E. L. Recent advancements in low cost solar cell processing. in *Proceedings of the 11th Photovoltaic Specialists Conference.* Vol. 1, p. 315 (1975).
3. Faddoul, R., Reverdy-Bruas, N., & Blayo, A. Formulation and screen printing of water based conductive flake silver pastes onto green ceramic tapes for electronic applications. *Mater. Sci. Eng. B Solid-State Mater. Adv. Technol.* **177,** 1053-1066 (2012).
4. Rane, S. B., Seth, T., Phatak, G. J., Amalnerkar, D. P., & Das, B. K. Influence of surfactants treatment on silver powder and its thick films. *Mater. Lett.* **57,** 3096-3100 (2003).
5. Rane, S. B., *et al.* Firing and processing effects on microstructure of fritted silver thick film electrode materials for solar cells. *Mater. Chem. Phys.* **82,** 237-245 (2003).
6. Faddoul, R., Reverdy-Bruas, N., & Bourel, J. Silver content effect on rheological and electrical properties of silver pastes. *J. Mater. Sci. Mater. Electron.* **23,** 1415-1426 (2012).
7. Nijs, J. F. , Szlufcik, J., Poortmans, J., Sivoththaman, S., & Mertens, R. P. Advanced manufacturing concepts for crystalline silicon solar cells. *IEEE Trans. Electron Devices.* **46,** 1948-1969 (1999).
8. Gomatam, R., & Mittal, K. L. *Electrically Conductive Adhesive.* CRC Press (2008).
9. Pospischil, M. *et al.* Investigations of thick-film-paste rheology for dispensing applications. *Energy Procedia.* **8,** 449-454 (2011).
10. Hoornstra, J., Weeber, A. W., De Moor, H. H., & Sinke, W. C. The importance of paste rheology in improving fine line, thick film screen printing of front side metallization. *Netherlands Energy Res. Found. ECN.* (1997).
11. Gilleo, K. Rheology and surface chemistry for screen printing. *Screen Print. Mag.* 128-132 (1989).
12. Lin, H. W., Chang, C. P., Hwu, W. H., & Ger, M. D. The rheological behaviors of screen-printing pastes. *J. Mater. Process. Technol.* **197,** 284-291 (2008).
13. Shiyong, L., Ning, W., Wencai, X., & Yong, L. Preparation and rheological behavior of lead free silver conducting paste. *Mater. Chem. Phys.* **111,** 20-23 (2008).
14. Reichl, H., & Feil, M. *Hybridintegration: Technologie und Entwurf von Dickschichtschaltungen.* Hüthig Verlag GmbH (1986).
15. Thibert, S. *et al.* Study of the high throughput flexographic process for silicon solar cell metallisation. *Prog. Photovoltaics Res. Appl.* **24,** 240-252 (2016).
16. Glunz, S. W., Mette, A., Richter, P. L., Filipovic, A., & Willeke, G. New concepts for the front side metallization of silicon solar cells. *21st Eur. Photovolt. Sol. Energy Conf.* 4-7 (2006).
17. Thibert, S. , Jourdan, J., Bechevent, B., Chaussy, D., Reverdy-Bruas, N., & Beneventi, D. Influence of silver paste rheology and screen parameters on the front side metallization of silicon solar cell. *Mater. Sci. Semicond. Process.* **27,** 790-799 (2014).
18. Pospischil, M. *et al.* Dispensing technology on the route to an industrial metallization process. *Energy Procedia.* **67,** 138-146 (2015).
19. Coussot, P. *Rheometry of pastes, suspensions, and granular materials: Application in Industry and Environment.* Wiley-interscience (2005).
20. Coussot, P. Rheophysics of pastes: a review of microscopic modelling approaches. *Soft Matter.* **3,** 528 (2007).
21. Zhou, H., Hong, J., Piao, L., & Kim, S.-H. Dual rheological responses in Ag pastes. *J. Appl. Polym. Sci.* **129,** 1328-1333 (2013).
22. Buscall, R., McGowan, J. I., & Morton-Jones, A. J. The rheology of concentrated dispersions of weakly attracting colloidal particles with and without wall slip. *J. Rheol. (N. Y. N. Y).* **37,** 621 (1993).
23. Kalyon, D. M., Yaras, P., Aral, B., & Yilmazer, U. Rheological behavior of a concentrated suspension: A solid rocket fuel simulant. *J. Rheol. (N. Y. N. Y).* **37,** 35-53 10.1122/1.550435 (1993).
24. Yilmazer, U., & Kalyon, D. M. Slip effects in capillary and parallel disk torsional flows of highly filled suspensions. *J. Rheol. (N. Y. N. Y).* **33,** 1197-1212 (1989).
25. Aral, B. K., & Kalyon, D. M. Effects of temperature and surface roughness on time-dependent development of wall slip in steady torsional flow of concentrated suspensions. *J. Rheol.* **38,** 957-972 (1994).
26. Persello, J., Magnin, A., Chang, J., Piau, J. M., & Cabane, B. Flow of colloidal aqueous silica dispersions. *J. Rheol. (N. Y. N. Y).* **38,** 1845-1870 (1994).
27. Pignon, F., Magnin, A., & Piau, J. M. Thixotropic colloidal suspensions and flow curves with minimum: Identification of flow regimes and rheometric consequences. *J. Rheol. (N. Y. N. Y).* **40,** 573-587 (1996).
28. Meeker, S. P., Bonnecaze, R. T., & Cloitre, M. Slip and flow in pastes of soft particles: Direct observation and rheology. *J. Rheol. (N. Y. N. Y).* **48,** 1295-1320 (2004).
29. Seth, J. R., Cloitre, M., & Bonnecaze, R. T. Influence of short-range forces on wall-slip in microgel pastes. *J. Rheol. (N. Y. N. Y).* **52,** 1241-1268 (2008).

30. Seth, J. R., Locatelli-Champagne, C., Monti, F., Bonnecaze, R. T., & Cloitre, M. How do soft particle glasses yield and flow near solid surfaces? *Soft Matter.* **8,** 140-148 (2012).
31. Meeker, S. P., Bonnecaze, R. T., & Cloitre, M. Slip and flow in soft particle pastes. *Phys. Rev. Lett.* **92,** 1-4 (2004).
32. Xu, C., Fieß, M., & Willenbacher, N. Impact of wall slip on screen printing of front-side silver pastes for silicon solar cells. *IEEE Journal of Photovoltaics.* **7**, 129-135 (2017).
33. Brummer, R. *Rheology Essentials of Cosmetic and Food Emulsions.* Springer Berlin-Heidelberg (2006).
34. Macosko, C. W. *Rheology Principles, Measurements, and Applications.* Wiley - VCH, New York (1994).
35. Dzuy, N. Q., & Boger, D. V. Yield stress measurement for concentrated suspensions. *J. Rheol. (N. Y. N. Y).* **27,** 321 - 349 (1983).
36. Cruz, F. Da, Chevoir, F., Bonn, D., & Coussot, P. Viscosity bifurcation in granular materials, foams, and emulsions. *Phys. Rev. E.* **66,** 1-7 (2002).